Kinetic Insights over a PEMFC Operating on Stationary and Oscillatory States

ARTICLE *in* THE JOURNAL OF PHYSICAL CHEMISTRY A · DECEMBER 2011

Impact Factor: 2.69 · DOI: 10.1021/jp205341w · Source: PubMed

3 AUTHORS:

Andressa Mota-Lima
Universidade Federal do Rio Grande do Norte
8 PUBLICATIONS **47** CITATIONS
SEE PROFILE

Ernesto R Gonzalez
University of São Paulo
97 PUBLICATIONS **2,630** CITATIONS
SEE PROFILE

Markus Eiswirth
Fritz Haber Institute of the Max Planck Society
123 PUBLICATIONS **3,704** CITATIONS
SEE PROFILE

THE JOURNAL OF PHYSICAL CHEMISTRY A

ARTICLE

pubs.acs.org/JPCA

Kinetic Insights over a PEMFC Operating on Stationary and Oscillatory States

Andressa Mota,*[,†,‡] Ernesto R. Gonzalez,[†] and Markus Eiswirth[‡,§]

[†]Instituto de Química de São Carlos, Av. Trab. Sancarlense 400, CEP 13560-970, São Carlos-SP, Brazil

[‡]Fritz-Haber-Institut der Max-Planck-Gesellschaft, Faradayweg 4-6, Berlin, Germany D-14195

[§]Ertl Center for Electrochemistry and Catalysis, GIST, Cheomdan-gwagiro 261, Buk-gu, Gwangju 500-712, South Korea

ABSTRACT: Kinetic investigations in the oscillatory state have been carried out in order to shed light on the interplay between the complex kinetics exhibited by a proton exchange membrane fuel cell fed with poisoned H_2 (108 ppm of CO) and the other in serie process. The apparent activation energy (E_a) in the stationary state was investigated in order to clarify the E_a observed in the oscillatory state. The apparent activation energy in the stationary state, under potentiostatic control, rendered (a) $E_a \approx 50-60$ kJ mol^{-1} over 0.8 V < E < 0.6 V and (b) $E_a \approx 10$ kJ mol^{-1} at E = 0.3 V. The former is related to the H_2 adsorption in the vacancies of the surface poisoned by CO and the latter is correlated to the process of proton conductivity in the membrane. The dependence of the period-one oscillations on the temperature yielded a genuine Arrhenius dependence with two E_a values: (a) E_a around 70 kJ mol^{-1}, at high temperatures, and (b) E_a around 10−15 kJ mol^{-1}, at lower temperatures. The latter E_a indicates the presence of protonic mass transport coupled to the essential oscillatory mechanism. These insights point in the right direction to predict spatial couplings between anode and cathode as having the highest strength as well as to speculate the most likely candidates to promote spatial inhomogeneities.

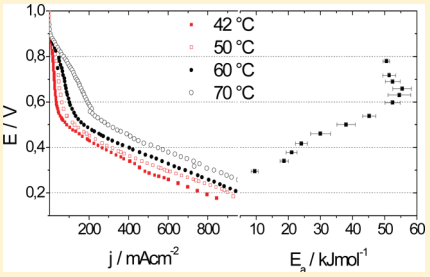

1. INTRODUCTION

A proton exchange membrane fuel cell (PEMFC) is an electrochemical device which couples two of the most studied electrochemical reactions: the hydrogen oxidation reaction (HOR) at the anode and the oxygen reduction reaction (ORR) at the cathode, by means of the protonic conduction of Nafion (the polymer membrane electrolyte). There is also a coupling by the electrons flowing from anode to cathode, but this process is not limiting. The presence of autosustained galvanostatic oscillations of the total PEMFC potential was experimentally observed for Pt-alloy catalysts.[1−7]

The origin of the potential oscillations in the PEMFC was assigned to the complex kinetics of hydrogen oxidation in the presence of CO[2−4] whenever the appropriated parameters are set up. In such conditions the core kinetic mechanism[8] links the CO adsorption and the CO oxidation (the so-called Langmuir−Hinshelwood (LH) mechanism) respectively to the positive and to the negative feedback on the anode overpotential.

From the mechanistic point of view, the oscillatory state in PEMFCs is predicted to be present in Pt alloys as well as pure Pt catalysts unless different ranges of parameters (for instance the carbon monoxide partial pressure, the applied current etc.) are required to establish the H_{opf} bifurcation. Platinum alloy makes alteration of the kinetics of CO adsorption and oxidation possible with the aim of making them slower and faster, respectively. Therefore, platinum alloying will alter the range of parameters that establish the H_{opf} bifurcation,[9] being the latter basically dependent on the rate constants of CO adsorption and oxidation. PEMFC oscillations on Pt−Ru nanoparticles are broadly reported[1−6] and have also recently been reported on palladium−Pt[7] alloy and pure Pt[10] nanocatalysts.

At the very beginning, when the first experimental PEMFC potential oscillation was reported,[1,2] investigation on the oscillatory PEMFCs was speeding up with the goal of building up electrochemical filters to purify reformate gases.[11−13] Simultaneously, more fundamental studies in PEMFC described the phase space dynamics for the Pt−Ru catalyst[4,5] accounting for time pattern of period one and two as well as aperiodic. Considering the spatially homogeneous case, the kinetic mechanism on the anode surface is enough to account for the dynamics of period one.[2−4] Nevertheless, the temporal pattern described in ref 5 requires an additional third degree of freedom from the mathematical point of view.[14] A possibility emerges whenever spatial coupling (by diffusion of species driving the instability)[15] is allowed for; that is, each electrochemical site is treated as being an oscillator which had temporal dependence on the coordinates of the system (for a survey of the nomenclature in the field, see ref 16). This issue was already debated in the 1990s. For instance, a mixed mode[17] was found in simulation when the phase transition on the surface of single crystals was modeled as being the third variable.[16,18] Christoph and Eiswirth[19] postulate a general framework to explain electrochemical pattern formation in a flat electrode, which has been recently applied by Kirsch et al.[20] to the fuel cell device.

Received: June 7, 2011
Revised: October 19, 2011

   dx.doi.org/10.1021/jp205341w | J. Phys. Chem. A XXXX, XXX, 000–000

Nevertheless, the same complex kinetic mechanism taking place on the electrode of a half cell (three electrode cell) and of a fuel cell device should have qualitative differences since both experimental approaches should have, in principle, different coupling between electrochemical sites along the electrode spatial coordinate. This last mentioned point will be discussed particularly in the end of this contribution. We aim to clarify the interplay between the oscillatory mechanism and the other kinetics process present in the FC. With this goal in mind, experimental kinetic investigations of sustained potential oscillations as well as in the stationary state were carried out.

2. EXPERIMENTAL METHODS

Commercial PtRu/C and Pt/C (20 wt %, E-TEK) were employed as anode (0.35 mg cm^{-2}) and cathode (0.4 mg cm^{-2}) catalysts, respectively. The catalyst structures consist of metal nanoparticles, around 3 nm,[21] anchored on carbon black particles whose diameter lays around 30−60 nm. A catalyst layer was prepared by brushing ink prepared by dispersing the catalysts with 0.96 mg cm^{-2} of Nafion in a mixture of alcohols. All of these procedures are described in a earlier publication.[22] Both 5 cm^2 diffusion electrodes and the previously treated membrane (Nafion 115) were hot pressed for 2 min, and the membrane/electrodes assembly (MEA) was prepared in that way a few minutes before carrying out the experiments. This procedure was adopted in order to reproduce the same dynamics of the pervious[4,5] works.

In order to produce a steady stationary state, the polarization curves were captured with the following procedure: a constant current or voltage (depending on the control mode) was applied and the respective voltage or current read after 5 s; this procedure avoids transients. The MEA operational parameters were controlled by a test station (Fuel Cell Technologies Inc.). The MEA operated with 200 sccm (standard cubic centimeters per minute) continuous flow of H_2 (with and without 108 ppm of CO as poison) and 50 sccm of water saturated O_2; both gases were saturated in water at the same temperature set up for the FC. Temperature and other control parameters were held constant over 1 h before each isothermal experiment. The protocol before the measurement includes the thermal activation[23] of the MEA at 70 °C for 3 h and isothermal measurements captured at cooling.

In order to investigate oscillatory dependence on temperature, a strategy to avoid different dynamic states was adopted (see experimental mapping of dynamic states in ref 5). The system maintained a dynamic state in period one by applying constant high values of current and anodic flow. The time series were recorded using a digital multimeter (Minipa, ET-2507) which was connected to the terminals of the cell. Before each isothermal measurement, anodic flux was held constant under low current over the time required to the fuel cell potential reached the lowest stable value. Therefore, the initial condition of the anodic surface corresponds to the maximum CO coverage. Departing from this initial condition, the system was pushed to the current values which delivered an oscillatory state.

Estimations of the E_a for the oscillatory regime consisted of evaluating the dependence of the oscillatory frequency under the inverse of the temperature, measuring the potential time series under galvanostatic control and then extracting the frequency. The dependence of the frequency on the temperature is a usual issue for biological systems.[24] Nevertheless, the temperature dependence of the oscillatory behavior of a fuel cell device has only recently been investigated.[2] This work systematically studies the oscillatory frequency dependence on temperature employing the knowledge gained from a physical chemical point of view.[25,26]

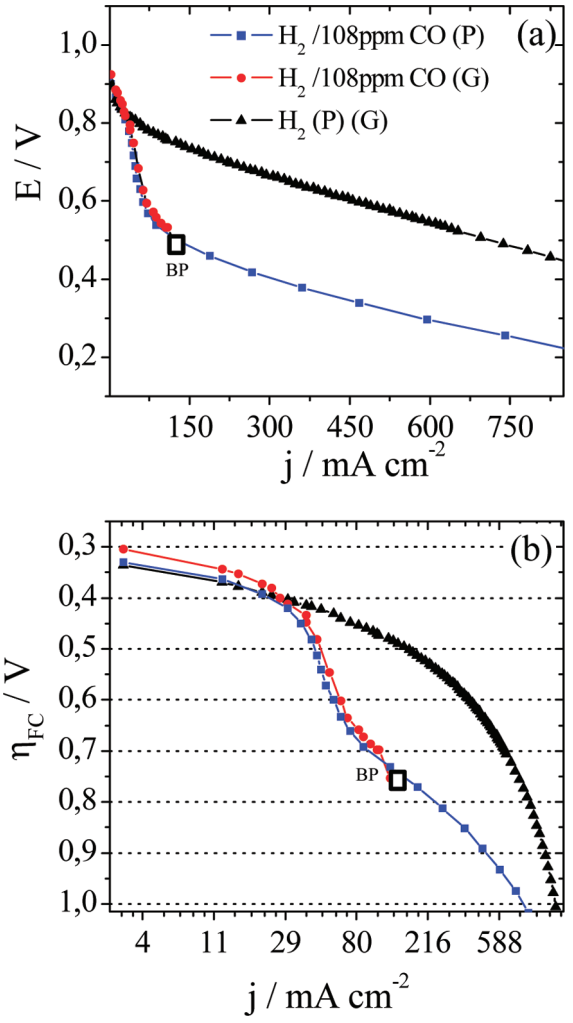

Figure 1. (a) Polarization curves under potentiostatic (P) and galvanostatic (G) control and (b) the same data in logarithmic representation but in terms of fuel cell overvoltage (η_{FC}). The erratic point due to pushing the FC further the H_{opf} bifurcation was omitted. Other conditions: Pt/C and PtRu/C as cathodic and anodic catalysts (0.4 and 0.35 mg cm^{-2}, respectively); 200 sccm of water saturated H_2 with 108 ppm of CO; 50 sccm of water saturated O_2; T_{cell}= 50 °C; Nafion 115. BF is the acronym for bifurcation point.

3. RESULTS AND DISCUSSION

3.1. Activation Energy in the Stationary State. Dissimilar behaviors of the polarization curve are displayed by the fuel cell anode catalyst PtRu/C fed with pure and poisoned H_2 (108 ppm of CO as poison) depending on the electrochemical mode of control, see Figure 1a. Stationary state under potentiostatic control (P) and the onset of an oscillatory regime in a branch of the galvanostatic (G) control profile were observed. A further current increase toward the bifurcation point turned the FC operation into the oscillatory regime whose experimental pairs current−potential were excluded from this graph to emphasize that the dynamics should be more properly characterized in terms of the respective experimental phase space.[5] However, the

dx.doi.org/10.1021/jp205341w |J. Phys. Chem. A XXXX, XXX, 000–000

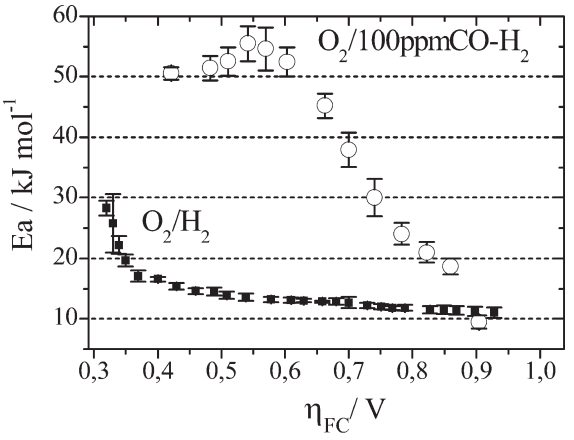

Figure 2. Activation energy (E_a) at the reference potential for H_2 feeding anode gases with and without CO. Other conditions: 45−75 °C temperature range; 50 sccm of water saturated O_2; 200 sccm of water saturated H_2. Bars mean the error for estimative of angular coefficient (from the linear curve j vs T^{-1}) multiplied by the gas constant (R).

same catalyst fed with pure H_2 displays the same profile for both cases of electrochemical control.

In order to describe the polarization curve in terms of the apparent activation energy (E_a), it was chosen to investigate the stationary state under potentiostatic mode in the presence of CO traces and also the stationary state displayed by the anode fed with pure H_2. The values of E_a found for the rate-determining step (rds) on the stationary regime were expected to clarify the E_a displayed in the oscillatory regime.

Figure 2 shows a kinetic description in the stationary state of the FC in terms of the apparent activation energy. The Arrhenius correlations between current and the reciprocal of the temperature were employed. As the polarization curve is a set of current−potential pairs, we represented the activation energy for each FC potential in terms of the respective FC overvoltage. For the cases of the FC fed with $|O_2||H_2|$ and $|O_2||H_2$,100 ppmCO|, the global reaction in the FC is taken into consideration

$$1/2O_2\ (g)\ +\ H_2\ (g) \rightarrow H_2O\ (g) \quad E^\circ = 1.23\ V \qquad (1)$$

The fuel cell overvoltage is introduced here as

$$\eta_{FC} = 1.23 - E_{FC} \qquad (2)$$

where E_{FC} reads the fuel cell voltage at a level of electrical current. The fuel cell overvoltage (η_{FC}) accounts for all kinds of overvoltage losses. This concept of fuel cell overvoltage is not strictly correct because overvoltage is defined for a single electrode process, i.e., the rationalization of how the electrode potential changes when a current passes. The FC is a device designed to promote global reaction 1 in an electrochemical way by splitting it into two half-reaction taking place over each one of the two electrodes separated by the Nafion membrane. Therefore, the fuel cell efficiency (and energy dissipation) does not depend uniquely on a single electrochemical process. Far from being a new concept, but rather a representation to emphasize the presence of an additional nonelectrochemical processes (ohmic drop of the membrane), the η_{FC} allows a more proper description of a device with a diversity of kinetic (and also dissipation) domains.

Facing the task of identifying the governing process in the stationary state, the Tafel diagram was employed as a base for comparison. It was obtained by plotting the polarization data of Figure 1a in a semilog form and chosen to represent the FC potential in terms of the overvoltage. It is possible to identify in Figure 1b regions of FC overpotential at which different mechanisms are operating.

We discuss in this section the process dictating the E vs j profile, Figure 1b, and correlate it with the respective values of activation energy, Figure 2. Activation energies available in the literature for the most important fuel cell elementary reactions as well as for protonic membrane conduction are compiled in Table 1. This table summarizes all the information useful for the discussion made ahead.

At first glance, the polarization curve seems to be dictated by a process with a large potential drop, but actually it is a wrong impression. The process having the lowest rate, known as the rate determining step (rds), constrains the flow of all series processes and has its E vs j profile assigned into the polarization curve. As a result there are domains of rds in the whole E vs j profile which could be kinetic domains of electrochemical control as well as mass transport control.

The first domain in both systems, $|O_2||H_2|$ and $|O_2||H_2$, 100ppmCO|, is a constraint due to the slow kinetics of the oxygen reduction reaction (ORR) at the smallest current densities in the polarization curve, which is better stressed in Figure 1b as being a linear region at FC overpotentials of less than 0.4 V.

It is well-known that, even at small current densities, the ORR displays a high overvoltage around 300 mV. When the model proposed by Ticianelli et al.[27] is fitted to the experimental data up to 350 mV, it yields the kinetics of charge transfer with a Tafel coefficient of 65 mV dec^{-1} which is in agreement with the value expected for the first electron transfer of the ORR. Thereby, estimation of E_a for η_{FC} at most 350 mV should yield the E_a related to the first electron transfer of the ORR. Estimated E_a, as seen in Figure 2, is 28 kJ mol^{-1} at 300 mV and it gradually decreases to a value of 18 kJ mol^{-1} at 400 mV.

The E_a found in the literature for the ORR either on single or polycrystalline platinum surfaces varies from 10 to 96 kJ mol^{-1}. In spite of this divergence, there is good agreement between the results in this work and those reported for the same reaction investigated in an operational PEMFC.[28,29] Thompson et al.[29] observed 25 kJ mol^{-1} at 310 mV which is close to our finding of 28 kJ mol^{-1} at 300 mV. Additionally, the same authors reported the higher overpotential, the lower E_a which is also observed in this work.

Pushing the overvoltage forward the RRO domain makes the FC enter in the second kinetic domain which has discernible characteristics depending on whether CO traces are present or absent in the fed hydrogen.

The second usual domain, found in the $|O_2||H_2|$ system, corresponds to the domain of the membrane protonic conduction, at fuel cell potentials (E_{FC}) lower than 0.7 V, see Figure 1a, or in other words, FC overpotentials larger than 0.4 V, see Figure 1b. When analyzing this overvoltage domain in Figure 2, the estimated E_a has values of 10−15 kJ mol^{-1}, which among all the E_a values taken from the literature (compiled in Table 1) for the conductivity in Nafion, seems to be in good agreement with E_a displayed by the particular case of Nafion with maximum water content (λ_{H_2O}), which reads $\lambda_{H_2O} = 14$. Also, the estimated E_a in this work is in agreement with E_a estimated from literature

dx.doi.org/10.1021/jp205341w |J. Phys. Chem. A XXXX, XXX, 000–000

Table 1. Activation Energies for Different Elementary Steps Found in a MEA Assembly[a]

surface/material	technique/electrolyte	E_a, kJ mol^{-1}	ref
	Hydrogen Oxidation Reaction (HOR)		
Pt(111)	VC of H_{upd} /0.05 M, H_2SO_4	40 @ θ = 0; 12.5 @ θ = 0.66	69
Pt(111)	VC of H_{upd}	42 @ θ = 0; 24 @ θ = 0.66	70
Pt/C	RDE/0.1 M H_2ClO_4	43	71
PtRu/C	PEMFC (H_2/air)/N112	34.6	72
	Oxygen Reduction Reaction (ORR)		
Pt(110), Pt(100), and Pt(111)	RDE/0.05 M, H_2SO_4	42 @ η = 0	73
Pt-poly	RDE/H_2SO_4, pH 1	30−25 @ 0.8 V; 22.7 @ η = 0	74
Pt-Nafion	special approach/P_{O_2} = 5 atm	28@ E < 0.75 V or η > 0.45	75
Pt/C	RRDE/0.5 M H_2SO_4 /0.5 M $HClO_4$	26 @ η = 0.35 V; 8 @ η = 0.35 V	76
Pt/C	RRDE/1 M CF_3SO_3H	19.12 @ E < 0.70 V 27.84 @ E < 0.85 V	77
Pt/C, Nafion -Pt(bulk)	channel flow/0.1 M $HClO_4$	38 @ η = 0.485	78
Pt/C	PEMFC	67 @ η = 0 38 @ η = 0.3 V 33 @ η = 0.35 V	28
Pt/C	PEMFC (H_2/air)/N117	25 @ η = 0.31 V	29
Pt-Nafion	DHE**/Nafion/Pt-disk	34 @ η = 0.23 V 54.7 @ E > 0.80 V	79
	N117	58.2 @ E < 0.80 V	
Pt/C	MEA Pt/C|PtRu-C	49 @ 100% RH, λ_{H_2O} = 14 55 @ 50% RH, λ_{H_2O}=	80
	Adsorption/Desorption of CO		
RuPt/C	QMS interface solid/gas	33,2	81
Pt/C (desorption)	CO/SV N112	28	60
Pt/C	QMS interface solid/gas	97,4	81
Pt - monocrystal	interface solid/gas	138@ θ = 0.7 46 @ θ = 0	82
	Oxidative Desorption of CO_{ad}		
Pt-Poly	TDP/0.05 M, H_2SO_4	101 @ θ= 0.95; 110@ θ = 0.75	83
Pt(111)	RDE/0.1 M NaOH	36 @ 0.3 V; 34 @ 0.6 V	70
Pt(111)	CO/SV/0.1 M, H_2SO_4	132	84
Pt(111) and Pt(100)	CO/SV 0.1 M, $HClO_4$	111.5; 122.5	85
	Protonic Conduction of Nafion		
N117	IS	9,6	86
N117	HFR	13.5	87
N115	modeling	14	33
N117	4-point HFR	2 @ λ_{H2O} = 14*	88
N117	HFR	14 @ λ_{H2O} = 13;* 9 @ λ_{H2O} = 20*	32
N117	HFR	22 @ λ_{H2O} = 2.2;* 10 @ λ_{H2O} = 14*	84
N212/N112	estimated from literature	7.19/11.11	30
N117/N115	estimated from literature	14.00 @ 0 mA cm^{-2} 10.85 @ 380 mA cm^{-2}	31

[a] RDE, rotatory disck electrode. HFR, high frequency resistance. IS, impedance spectroscopy. CO/SV, CO stripping voltametry. RRDE, rotating ring disk electrode. QMS, quadrupole mass spectroscopy. TPD, temperature programmed desorption. N, Nafion membrane in the thickness: 117, 115, and 112. ** DHE, dynamic hydrogen electrode. * Membrane water content.

data[30,31] for the membrane resistance measured in an operational fuel cell employing water saturated gases similar to the device employed in this work.

Halseid et al.[32] stressed that E_a for the conductivity in Nafion is a function of the membrane water content. The dispersion of E_a values (check Table 1) follows a tendency whenever the water content is taking account. The experimental dependence of the membrane water content on the water activity in the vapor phase[33,34] allows us to read λ_{H_2O} = 14 for saturated water vapor (the maximum water content) and reads λ_{H_2O} < 14 for water

dx.doi.org/10.1021/jp205341w |J. Phys. Chem. A XXXX, XXX, 000–000

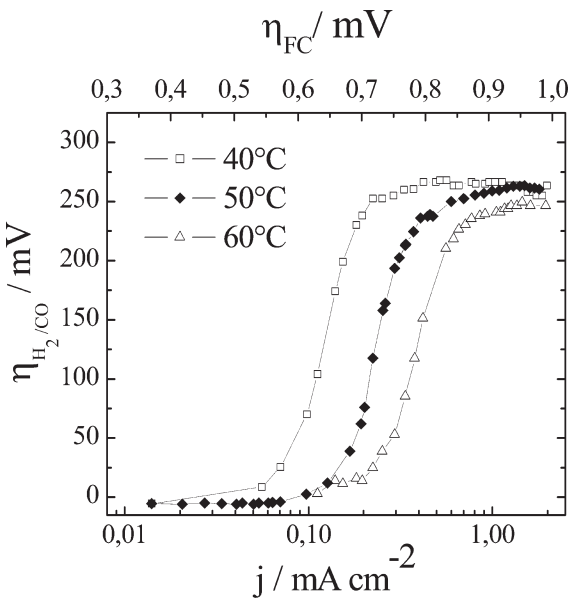

Figure 3. Anodic polarization curve. Pt/C and PtRu/C as cathodic and anodic catalyst (0.4 and 0.35 mg cm^{-2}, respectively); 200 sccm of water saturated H_2 with 108 ppm of CO; 50 sccm of water saturated O_2; T_{cell} = 50 °C; Nafion 115.

partial pressure smaller than the saturation point. With this in mind, we deduce that in our experiments the E_a of the membrane has value of $\lambda_{H_2O} = 14$. Actually, the E_a agrees well with the E_a at maximum Nafion hydration. In conclusion, at FC overpotentials induced by the membrane resistivity, the rates of both the ORR and the HOR (hydrogen oxidation reaction) are intrinsically faster than the conduction in the membrane. Thereby, the total current of the FC is constrained by the low capability of the membrane to sustain a high flow of protons . The conclusion which could be drawn is that the coupling between the ORR and the HOR is intermediated by means of a constant flow of protons. Or in other words, the membrane drives the stationary regime of drain and source of protons on both anodic and cathodic reactions.

The third and fourth overpotential domains are present for the case of $|O_2||H_2$,100ppmCO| at the overpotential intervals 0.4 V < η_{FC} < 0.7 and at η_{FC} > 0.7 V, respectively, see Figure 1b. The first attempt to understand the rds of the anodic process when the anode is fed with H_2/CO is done by analyzing the anodic overvoltage (η_a) profile against the current. This plot is done by making the difference between the fuel cell overvoltage for the cases of pure and impure hydrogen and applying eq 2 to eq 3

$$\eta_{FC} = \eta_a + \eta_c + IR_{mem} \quad (3)$$

where the fuel cell overvoltage is the sum of the overvoltage belonging to the anodic process (η_a), cathodic process (η_c), and ohmic potential drop due to the resistive component of the membrane (R_{mem}) and assuming two points: the cathode overvoltage remains the same for the pure and impure anodic gas and the membrane resistance does not depend on the current neither in the presence of poison; thereby, η_a due to the presence of poison is calculated as

$$\eta_a = E_{FC}(|PtRu|H_2|) + E_{FC}(|PtRu|H_2, 100ppmCO|) \quad (4)$$

Doing the same for the data from Figure 1a, the Tafel diagram for the anodic reaction is shown in Figure 3. The typical polarization curve displays the existence of three characteristic regions.[35] The first region below 20 mV has a profile dictated by the fast HOR kinetics, more precisely the Volmer step;[36] the second region accounts for a huge range of the total overvoltage, i.e., 20 mV > η_a > 250 mV and finally, the third region above η_a > 250 mV.

Concerning the huge increase in polarization in the range 0.4 V < η_{FC} < 0.7 V (20 mV > η_a >250 mV), the fitting of the Butler−Volmer equation is unfeasible for this domain; that is, the kinetics is controlled by a nonelectrochemical process. On the surface, the CO equilibrium coverage is accomplished and the HOR is allowed into the vacancies of the CO carpet. As the HOR is the current carrier the rds should be coupled in series with the HOR. Schmidt et al.[37] suggest CO adsorption/desorption-controlled vacancies for this region of the infinite Tafel coefficient. This reasoning considers the main poisoning effect as the site exclusion for the reactants. Following this reasoning, Camara et al.[35] and Lee et al.[36] raised the hypothesis that the Tafel step is the rds. Subsequently, the authors suggest the presence of a limiting current controlled by the rate of H_2 adsorption.

More details about the kinetics of the HOR in the presence of CO in the huge range of anode overvoltage emerge from the powerful impedance technique. The study of the HOR in the presence of CO by the EIS technique in a small fuel cell identified three processes:[38,39] the HOR charge transfer process, H_2 adsorption/diffusion on the surface and the proton hydration step. The presence of CO promotes a slowdown of the charge transfer rate for the HOR.[38−40] This event is assigned to the "interaction effect" as claimed by Meland and Kjelstrup after discovering that the time relaxation for the HOR is the unique process to increase drastically in the presence of CO.[39] Such scenario was explained using the argumentation of CO polarization on the surface. This fact was exploited by Stonehart and Kohlmayr[41] who observed a strong decrease of the kinetic constant for the HOR whenever increasing CO coverage. In contrast, the authors did not observe any impact of the arsenic coverage (another poison species) on the kinetics of the HOR. In summary, the kinetic parameters do not depend on the electrochemical area therefore it should also be independent of the poison coverage if the poison assumes solely the site exclusion effect. However, this is a false sentence for the CO poising case.

According to the rationalization above, the E_a of 50−60 kJ mol^{-1} corresponds to the adsorption of hydrogen from the gas phase on the poisoned surface. The activation energy for H_2 adsorption, around 40 kJ mol^{-1}, on bare Pt single crystals is in good agreement with the case of Pt nanocatalysts (see Table 1). The effect of Pt alloys probably does not alter the interaction between the hydrogen ion and the surface since the E_a for both pure and Pt alloys are not much different. Concerning the presence of trace of CO in the hydrogen gas, we believe the E_a will depend on the interaction between H_{ads} and CO_{ads} since H_2 adsorption actually depends on the hydrogen coverage for experiments with single crystal (check table 1). Since H and CO have a repulsive interaction[42] the value of E_a found here, around 50−60 kJ mol^{-1}, could not explain this interestingly higher value compared to the nonpoisoned PtRu/C (Table 1).

Analyzing the region η_{FC} > 0.7 V (or η_a > 250 mV) in Figure 5, Tafel coefficient b = 110 mV dec^{-1} is obtained which is similar to the experimental findings assumed for the LH mechanism.[37] Such a coincidence still does not clarify the rds imposed on the main current which is still supplied by the HOR. More probably, this coincidence points toward the kinetics of the CO

dx.doi.org/10.1021/jp205341w |J. Phys. Chem. A XXXX, XXX, 000–000

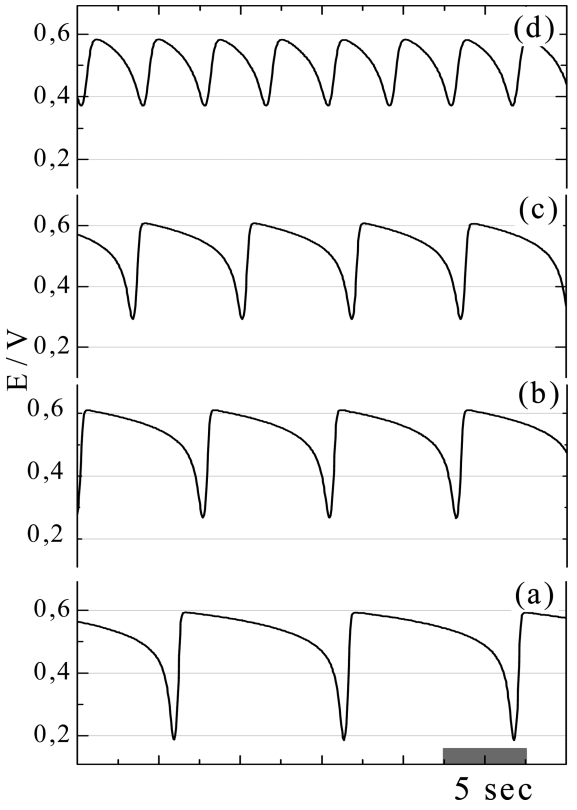

Figure 4. Potential time series of the fuel cell operating with 200 sccm of H_2-100ppmCO, constant current, j = 325 mA cm^{-2}, at temperatures (a) 36, (b) 50, (c) 56, and (d) 65 °C.

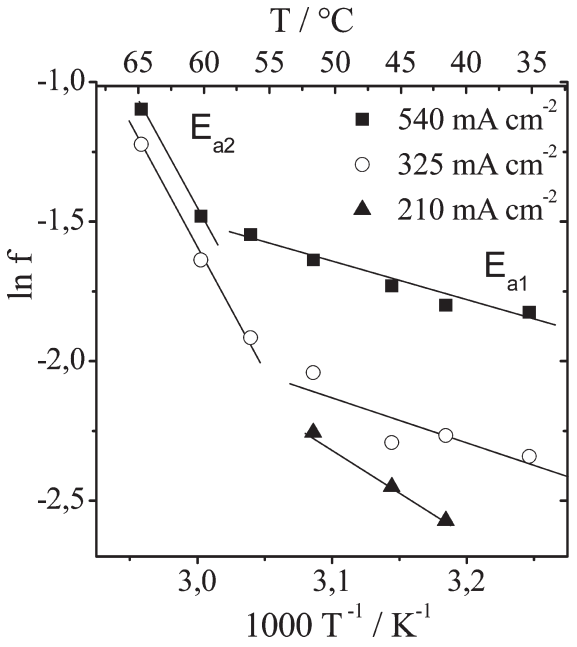

Figure 5. Effect of temperature on the oscillatory frequency of the FC operating in galvanostatic mode. Frequency calculated for the time series, one of them was depicted in Figure 4.

oxidation-controlled vacancies as already described by others.[37] In such a range, instead of being constant, the estimated E_a progressively decreases to ~10 kJ mol^{-1}. This last value is characteristic of the membrane conductivity. Finally, the values of E_a for CO adsorption, desorption and oxidation are shown in Table 1 in order to confirm the lack of agreement among them and the estimated E_a in this work for the considered range of overvoltage. It is credited that the system goes back to the kinetic control of the membrane at high values of the current.

3.2. Activation Energy in the Oscillatory State. A typical set of potential time series is shown in Figure 4. Globally, the higher the temperature is, the shorter the oscillatory period is. Nevertheless, a temperature higher than 75 °C makes the oscillation disappear which is in agreement with Zhang et al.[3] observations for similar operating conditions. Figure 5 shows the dependence of the oscillatory frequency on temperature. Interestingly, the frequency shows a dependence on temperature which could be approximated to two regions of Arrhenius dependence at low and high temperatures. This behavior is clearer at intermediate currents, *e.g.* 325 mA/cm^{-2}. Considering those two regions, the apparent E_a for each current region is presented in Table 2. The E_a calculated for different levels of current at low temperatures was 12−25 kJ mol^{-1}. Moreover, before the oscillatory regime disappears due to the temperature increase, E_a switches to 70 kJ mol^{-1}.

The oscillatory state does not have a unique elementary step as rate limiting step but it actually has a regulation of its frequency dictated by the time scale of essential feedback loops. Ruoff[25] discussed the frequency independence-temperature observed on the BZ reaction based on the effect of antagonistic balance

Table 2. Activation Energies for the Oscillatory Regime

current, mA/cm^{-2}	E_{a1}, kJ mol^{-1}	E_{a2}, kJ mol^{-1}
540	12.33 ± 1.2	71.60
325	14.25 ± 5.8	71.44 ± 4.1
210	26.81 ± 0.7	

between positive and negative feedback loops which could render anomalous behavior such as anti-Arrhenius and temperature compensation. It means, essentially, that the oscillatory period increases whenever the rate constant of the positive feedback loop rises. On the other hand, the period decreases whenever the negative feedback rate constant increases. So, the period dependence on temperature will account for the antagonistic balance. Later, Aase and Ruoff[43] systematically compiled experimental findings in a mathematical kinetic basis which reads

$$\frac{\partial \ln \omega}{\partial T} = \frac{1}{RT^2}\left[\sum^{n^+} C_i E_i - \sum^{n^-} C_i E_i\right] \quad (5)$$

where ω represents the oscillation frequency, T is the temperature, R is the gas constant, E_i is the activation energy of the i elementary step, and n represents a considered elementary step belonging to the positive (n^+) and negative (n^-) feedback loop. In order to simplify all subsequent analysis, the nonthermodynamic parameters were rewritten as a constant C_i[44]

$$C_i = k_i \left| \left(\frac{\partial \ln \omega}{\partial \ln k_i} \right)_T \right| \quad (6)$$

The sign of C_i depends on the derivative $\partial \ln \omega / \partial \ln k_i$.[44] The constant C_i has a negative sign when the elementary step i belongs to the negative loop because an increase in the rate constant of step i produces a shorting in the period. The same

dx.doi.org/10.1021/jp205341w |J. Phys. Chem. A XXXX, XXX, 000–000

rationalization for the positive feedback produces the opposite behavior and so, the positive sign is in front of the positive sum. Therefore, in eq 5, the constant C_i is analyzed in terms of the modulus value since the sign of this constant has already been taken into consideration in this expression. The absolute value of C_i is a key point in understanding E_a in the oscillatory regime. It informs the contribution of each elementary step (belonging to essential variables of the kinetic oscillator) on the oscillatory activation energy.

Notably, only the Arrhenius dependence was observed on the surface poisoned by CO as seen in this work; that is, temperature compensation was absent. Such unusual phenomenon happens whenever the time scales of positive and negative feedback loops have the same order of magnitude. These requirement seems to be fulfilled for most of the experimental potential-time series observed during the complex electro-oxidation of small organic molecules such as ethylene glycol[45] and formic acid[46] on polycrystalline surfaces. On the other hand, the electro-oxidation of methanol[47] and also the electro-oxidation of hydrogen in the presence of CO, seen in this work, produced genuine Arrhenius behavior. The slow step of CO adsorption on the catalyst surface (time scale of positive feedback) is very dissimilar compared to the fast scale of the Langmuir−Hinshelwood mechanism and therefore Arrhenius dependence should be expected. In terms of mathematical language, it means that there exists one coefficient C_i which has the largest numerical[26] value exist. As a result, Arrhenius behavior appears displaying E_a smoothly different from E_a characteristic of such an elementary step. In agreement with this reasoning, the oscillatory E_a value of 70 kJ mol^{-1}, seen at high temperatures, is sparsely spread compared to those found in a stationary state, i.e., 50−60 kJ mol^{-1} for the H_2 adsorption on a surface poisoned by CO.

Additionally, the findings of this work shed light in the results of Kadyk et al.[10] The authors found oscillatory frequency equal to 40 kJ mol^{-1}. This value is interpreted as being related to the hydrogen adsorption on the platinum surface. Actually, this value is in agreement with the one summarized in table 1.

Interestingly, our experimental values of E_a around 10−15 kJ mol^{-1}, at low temperatures, uncover the real situation concerning the coupling of the anode oscillatory mechanism and those other series processes inside the FC system.

The protonic conduction of the membrane, as observed in the stationary state of the FC, has characteristic values of the E_a around 10−15 kJ mol^{-1} which are similar to those found for the oscillatory regime at low temperatures. This unexpected E_a for low temperatures induces the idea that the Nafion protonic transport process should be coupled to the essential oscillatory mechanism of the HOR in the presence of CO. Actually, this indicates that the anodic oscillatory mechanism should be coupled to the flow of protons in the membrane. Even though the adsorption of CO and its subsequent removal by the LH mechanism happens parallel to the hydrogen electroxidation, it is the latter the main current carrier sustaining the anodic current. This also suggests that the HOR mechanism is related to the oscillatory rds. As the hydrogen electroxidation has the fastest kinetics of charge transfer, the period is mainly determined by hydrogen adsorption on the holes of the CO carpet for the results obtained by Kadyk[10] as well as mainly determined by the slow removal of protons from the interface catalyst/membrane, being the rate established by the proton conduction of the membrane, for the results of this work. It should be mentioned that this argumentation stands up for period one oscillation. We would extend the analysis for period two if the range of parameters were accessible at different temperatures.

3.3. Considerations about Instabilities in Two Modes of Control: Potentiostatic Control and External Resistance. Potentiostatic kinetic instability requires high resistance coupled with the interfacial kinetics as established by Koper.[48] The ohmic drop due to membrane resistance is the key point to define onset of the bifurcation point where the potentiostatic oscillation is seen. In this work, we only find stationary behavior in potentiostatic mode. The potentiostatic oscillation in the H_2/CO system requires high resistance of the Nafion hence an increase in the thickness of the Nafion (another way would be decreasing the intrinsic conductivity) could lead to some kinetic instability in potentiostatic mode. So far, the electrolyte conductivity was assumed to be constant everywhere for the instabilities in the half electrode which does not seem to be the case for the Nafion conductivity in the fuel cell device. In this case, the instability analyses of the kinetics should be made locally allowing for the local value of the membrane resistance.

The other mode of fuel cell operation is made by a adjusting an external resistance connected to the terminals of the cell. In this mode, there is a complete lack of external control and the potential and the current adjust themselves freely. In this mode of control, simultaneous current and potential oscillation was seen in the presence of the mixture H_2/CO as reported by Vayenas et al.[49,50] This operation mode of controlling the fuel cell has no analogy with the case of the half cell.

3.4. Consideration about Spatial Coupling of the Fuel Cell Electrochemical Oscillator and Other Nonlinear Phenomenon. The theoretical treatment of the pattern formation[19,51] in a single electrode includes a coupling of different electrochemical sites by means of the electrical field. Departing from the general solution of Laplace's equation for the electrochemical electrolyte,[19] the inhomogeneities of the potential for a single electrode are rationalized in terms of the concept of spatial coupling function. Nevertheless, there are particular differences in the treatment of the electric field coupling in the case of the fuel cell: the counter electrode is close to the working electrode; therefore, the coupling between two electrodes could not be neglected. About this concern, a comment is done in the paragraph below.

The coupling between anode and cathode is the candidate to have the highest strength as we argue ahead. The thickness of the membrane regulates the potential gradient between cathode and anode which is constant everywhere in the homogeneous case. As soon as a local inhomogeneity in the potential on the electrode appears, the average gradient between cathode and anode changes. Nevertheless, a negligible flux of protonic current to equalize inhomogeneities appears in the direction parallel to the electrode since the thickness of the membrane is 4 orders of magnitude (in our experiments) smaller than its perimeter. This geometry allows for a much stronger potential field between anode and cathode compared to potential gradient along a single electrode. As a consequence, electrochemical sites along the electrode have an electric coupling strength of zero with sites which are located at distances of three times the length of the membrane thickness, we would assume. For this geometry, the higher the length of separation between two spatial positions is, the shorter the coupling strength is. This is confirmed by the insights of this work which indicates the migration of protons through the Nafion as being the rate determining step in the oscillatory regimen i.e. the flow of protonic current in the

dx.doi.org/10.1021/jp205341w |J. Phys. Chem. A XXXX, XXX, 000–000

direction of the membrane thickness is the majority current. In such a scenario, the electrical field does not introduce coupling by protonic current along the anode surface as was early considered in modeling.[20]

The fuel cell accounts for other possibilities concerning the spatial inhomogeneities, which are absent in all sorts of theoretical treatment[19,52−54] and experimental approaches[55−57] for a flat electrode. The anode structure adds a coupling between different sites by means of the gas phase. The adsorption and oxidation of CO at the beginning of the flow channel allows for depletion of CO partial pressure (P_{CO}) and increase the CO_2 partial pressure (P_{CO_2}) at the end of the channel. The depletion of fuel[58] and water[59] along the serpentine flow channels in a PEMFC has already reported. The variation of the gas phase composition, along the serpentine channel, brings about some possibility for the spatial inhomogeneity in the potential. For instance, the P_{CO} is the critical parameter for Hopf bifurcation whose changing along the spatial coordinate is a candidate to add spatial variation of the level of local current required to the appearance of the bifurcation.

The second possibility for spatial inhomogeneity rises from depletion of the water partial pressure (P_{H_2O}) along the channel which could give rise to inhomogeneities of the proton conductivity along a position on the electrode surface since the Nafion conductivity has a strong dependence on factors such as the water uptake.[32,60,61] Therefore, the spatial variation of the Nafion conductivity is considered to be the most likely candidate to add spatial variations of the coupling between anode and cathode.

Finally, it is known that the oscillation is a sort of complex behavior allowed for electrochemical instability but the fuel cell displays another nonlinear events (see ref 62 for survey) whose kinetics does not necessary pass through some bifurcation. Among the other nonlinear events in the fuel cell, the most investigated is the multiplicity in the polarization curve. This comma shape E vs I curve allows for two levels of potential for the same level of current. Two researcher groups reached independently complementary conclusions. Katsaounis et al.[49,63,64] considered the nonlinear variation of the total fuel cell resistance as being a result of the nonlinear intrinsical conductivity of the membrane with the fuel cell potential under low hydrogen partial pressure (P_{H_2}). Moreover, the authors proposed a mechanism of proton conduction based on the two fundamental processes:[65] protons tunneling on the surface of the nanopores (compact area of the polymeric chair) and the migration into the aqueous phase of the micropores (swelling areas of the polymeric chair). Simultaneously, Schneider et al.[66,67]clarified the spatial aspect related with the comma shape curve by employing the locally resolved impedance spectroscopy. The authors identified an NDR located at the end of the gas flow field[66] as well as in the region between the tracks of the graphite plate (lands)[67] which displayed locally a comma shape curve and local NDR was explained as a direct consequence of down the channel inhomogeneities: changes in the fuel or water concentrations. Further, the authors argue that the local current at the end of the channel is lower than the total galvanostatic current[68] which we believe to be a perfect explanation for the local NDR. Although Schneider et al. do not discuss the results of Katsaounis et al., we believe (particularly one of the authors) that taking together both works corroborates to the follow conclusion: the macroscopic nonlinear behavior of the total fuel cell resistance is a severe consequence of local NDR somewhere in the course of the gas flow field caused by the low electro-kinetic activity. The argument in favor of the Nafion conductivity dependence on electro-kinetic activity lays on the fact that the charge carrier density (density of proton, in this case) is regulated by the HOR. As a conclude, the local comma shape should be a direct consequence of the Nafion conductivity dependent on the local depletion of the water partial pressure (P_{H_2O}) by means of the water uptake as well as on the local depletion of the oxidant fuel by means of the electro-kinetics carrier generation. This reinforces the idea of a spatial inhomogeneous Nafion conductivity which we exploit above.

4. CONCLUSIONS

The polarization curve of a PEMFC was described by the first time in terms of the activation energies displayed by the rds. The polarization curve for the FC fed with pure gases ($|O_2||H_2|$) yielded two domains of characteristic E_a due to the ORR kinetics and due to the proton conduction inside the membrane. The stationary polarization curve for the FC fed with impure gases ($|O_2||H_2$,100ppmCO|) yielded also two domains of characteristic E_a. Under potentiostatic control, it rendered (a) $E_a \approx 50-60$ kJ mol^{-1} over 0.4 V < η_{FC} < 0.6 V which represents the adsorption of hydrogen from the gas phase on the poisoned surface; and (b) $E_a \approx 10$ kJ mol^{-1} at η_{FC} = 0.9 V due to the mechanism of proton conduction in the membrane.

The knowledge gained whit the E_a in the stationary state clarified the values found in oscillatory state. Interestingly, the experimental value of E_a of 10−15 kJ mol^{-1} for the oscillatory regime, at low temperatures, uncovers the real situation concerning the coupling of the anode oscillatory mechanism and those other series processes inside the FC system. Hence, the discussion about the most feasible spatial couplings inside the fuel cell includes: coupling between cathode and anode as well as coupling of the electrode site through the gas phase along the gas channel. Furthermore, Nafion proton conductivity should couple cathode and anode with the highest strength as supported by the results of this work. On the other hand, inhomogeneities in composition of the gas phase along the gas channel bring about a possibility of coupling different sites along the anode surface. Furthermore, spatial variation of the Nafion conductivity is considered to be the most likely candidate to add spatial variations of the coupling between anode and cathode.

AUTHOR INFORMATION

Corresponding Author
*E-mail: mota@fhi-berlin.mpg.de.

ACKNOWLEDGMENT

The authors thank the comments from one of the reviewer. A. M. thanks CNPq (no.142739/2007-3) and CAPES (1270/10-9) for scholarships as well as Prof. Edson Ticianelli for fruitful discussion.

REFERENCES

(1) Murthy, M.; Esayian, M.; Hobson, A.; MacKenzie, S.; Lee, W.-k.; Van Zee, J. W. *J. Electrochem. Soc.* **2001**, *148*, A1141–A1147.
(2) Zhang, J.; Datta, R. *J. Electrochem. Soc.* **2002**, *149*, A1423–A1431.
(3) Zhang, J.; Fehribach, J. D.; Datta, R. *J. Electrochem. Soc.* **2004**, *151*, A689–A697.

(4) Mota, A.; Lopes, P. P.; Ticianelli, E. A.; Gonzalez, E. R.; Varela, H. *ECS Trans.* **2009**, *25*, 81–89.
(5) Mota, A.; Lopes, P. P.; Ticianelli, E. A.; Gonzalez, E. R.; Varela, H. *J. Electrochem. Soc.* **2010**, *157*, B1301–B1304.
(6) Lu, H.; Struckmann, L. R.; Rauschenbach, R. H.; Sundmacher, K. *Top. Catal.* **2008**, *51*, 89–97.
(7) Lopes, P. P.; Ticianelli, E. A.; Varela, H. *J. Power Sources* **2011**, *196*, 84–89.
(8) Eiswirth, M.; Bürger, J.; Strasser, P.; Ertl, G. *J. Phys. Chem.* **1996**, *100*, 19118–19123.
(9) Reichert, C.; Starke, J.; Eiswirth, M. *J. Chem. Phys.* **2001**, *115*, 4829–4838.
(10) Kadyk, T.; Kirsch, S.; Hanke-Rauschenbach, R.; Sundmacher, K. *Electrochim. Acta* **2011**.
(11) Zhang, J.; Datta, R. *J. Electrochem. Soc.* **2005**, *152*, A1180–A1187.
(12) Hanke-Rauschenbach, R.; Weinzierl, C.; Krasnyk, M.; Rihko-Struckmann, L.; Lu, H.; Sundmacher, K. *J. Electrochem. Soc.* **2009**, *156*, B1267–B1275.
(13) Lu, H.; Rihko-Struckmann, L.; Hanke-Rauschenbach, R.; Sundmacher, K. *Electrochim. Acta* **2009**, *54*, 1184–1191.
(14) Hilborn, R. *Chaos and Nonlinear Dynamics: An Introduction for Scientists and Engineers*; Oxford University Press: New York, 2001.
(15) Murray, J. D. *Mathematical Biology*; Springer-Verlag: Berlin, Germany, 1993.
(16) Eiswirth, R. M.; Krischer, K.; Ertl, G. *Appl. Phys. A: Mater. Sci. Process.* **1990**, *51*, 79–90.
(17) Krischer, K.; Lübke, M.; Eiswirth, M.; Wolf, W.; Hudson, J. L.; Ertl, G. *Phys. D* **1993**, *62*, 123–133.
(18) Krischer, K.; Eiswirth, M.; Ertl, G. *J. Chem. Phys.* **1992**, *96*, 9161–9172.
(19) Christoph, J.; Eiswirth, M. *Chaos* **2002**, *12*, 215–230.
(20) Kirsch, S.; Hanke-Rauschenbach, R.; Sundmacher, K. *J. Electrochem. Soc.* **2011**, *158*, B44–B53.
(21) Vogel, W. *J. Phys. Chem. C* **2008**, *112*, 13475–13482.
(22) Paganin, V. A.; Ticianelli, E. A.; Gonzalez, E. R. *J. Appl. Electrochem.* **1996**, *26*, 297–304.
(23) Xua, Z.; Qi, Z.; Hec, C.; Kaufmand, A. *J. Power Sources* **2006**, *156*, 315–320.
(24) Hastings, J. W.; Sweeney, B. M. *Proc. Natl. Acad. Sci.* **1957**, *43*, 804–811.
(25) Ruoff, P. *J. Interdiscipl. Cycle Res.* **1992**, *23*, 92–99.
(26) Ruoff, P. *Phys. D* **1995**, *84*, 204–211.
(27) Ticianelli, E. A.; Derouin, C. R.; Redondo, A.; Srinivasan, S. *J. Electrochem. Soc.* **1988**, *135*, 2209–2214.
(28) Neyerlin, K. C.; Gu, W.; Jorne, J.; Gasteiger, H. A. *J. Electrochem. Soc.* **2006**, *153*, A1955–A1963.
(29) Thompson, E. L.; Jorne, J.; Gasteiger, H. A. *J. Electrochem. Soc.* **2007**, *154*, B783–B792.
(30) Fernandes, A. C.; Ticianelli, E. A. *J. Power Sources* **2009**, *193*, 547–554.
(31) Freire, T. J. P.; Gonzalez, E. R. *J. Electroanal. Chem.* **2001**, *503*, 57–68.
(32) Halseid, R.; Vie, P. J. S.; Tunold, R. *J. Electrochem. Soc.* **2004**, *151*, A381–A388.
(33) Thampan, T.; Malhotra, S.; Tang, H.; Datta, R. *J. Electrochem. Soc.* **2000**, *147*, 3242–3250.
(34) Springer, T. E.; Zawodzinski, T. A.; Gottesfeld, S. *J. Electrochem. Soc.* **1991**, *138*, 2334–2342.
(35) Camara, G. A.; Ticianelli, E. A.; Mukerjee, S.; Lee, S. J.; McBreen, J. *J. Electrochem. Soc.* **2002**, *149*, A748–A753.
(36) Lee, S. J.; Mukerjee, S.; Ticianelli, E. A.; McBreen, J. *Electrochim. Acta* **1999**, *44*, 3283–3293.
(37) Schmidt, T. J.; Gasteiger, H. A.; Behm, R. J. *J. Electrochem. Soc.* **1999**, *146*, 1296–1304.
(38) Kim, J.-D.; Park, Y.-I.; Kobayashi, K.; Nagai, M.; Kunimatsu, M. *Solid State Ionics* **2001**, *140*, 313–325.
(39) Meland, A. K.; Kjelstrup, S. *J. Electroanal. Chem.* **2007**, *610*, 171–178.
(40) Wagner, N.; Schulze, M. *Electrochim. Acta* **2003**, *48*, 3899–3907.
(41) Stonehar., P; Kohlmayr, G. *Electrochim. Acta* **1972**, *17*, 369–382.
(42) Roman, T.; Nakanishi, H.; Kasai, H. *Phys. Chem. Chem. Phys.* **2008**, *10*, 6052–6057.
(43) Aase, S. O.; Ruoff, P. *J. Math. Biol.* **2008**, *56*, 279–292.
(44) Ruoff, P. *Naturwissenschaften* **1994**, *81*, 456–459.
(45) Sitta, E.; Nascimento, M. A.; Varela, H. *Phys. Chem. Chem. Phys.* **2010**, *12*, 15195–15206.
(46) Nagao, R.; Epstein, I. R.; Gonzalez, E. R.; Varela, H. *J. Phys. Chem. A* **2008**, *112*, 4617–4624.
(47) Carbonio, E. A.; Nagao, R.; Gonzalez, E. R.; Varela, H. *Phys. Chem. Chem. Phys.* **2009**, *11*, 665–670.
(48) Koper, M. T. M. *Electrochim. Acta* **1992**, *37*, 1771–1778.
(49) Katsaounis, A.; Balomenou, S.; Tsiplakides, D.; Brosda, S.; Neophytides, S.; Vayenas, C. G. *Appl. Catal. B: Environ.* **2005**, *56*, 251–258.
(50) Sapountzi, F. M.; Divane, S. C.; Tsampas, M. N.; Vayenas, C. G. *Electrochim. Acta* **2011**, *56*, 6966–6975.
(51) Krischer, K. *J. Electroanal. Chem.* **2001**, *501*, 1–21.
(52) Krischer, K. *J. Electroanal. Chem.* **2001**, *501*, 1–21.
(53) Siegmeier, J.; Baba, N.; Krischer, K. *J. Phys. Chem. C* **2007**, *111*, 13481–13489.
(54) Kiss, I. Z.; Pelster, L. N.; Wickramasinghe, M.; Yablonsky, G. S. *Phys. Chem. Chem. Phys.* **2009**, *11*, 5720–5728.
(55) Kiss, I. Z.; Brackett, A. W.; Hudson, J. L. *J. Phys. Chem. B* **2004**, *108*, 14599–14608.
(56) Kiss, I. Z.; Wang, W.; Hudson, J. L. *J. Phys. Chem. B* **1999**, *103*, 11433–11444.
(57) Kiss, I. Z.; Wang, W.; Hudson, J. L. *Phys. Chem. Chem. Phys.* **2000**, *2*, 3847–3854.
(58) Schneider, I. A.; Kramer, D.; Wokaun, A.; Scherer, G. G. *Electrochem. Commun.* **2007**, *9*, 1607–1612.
(59) Schneider, I. A.; Kuhn, H.; Wokaun, A.; Scherer, G. G. *J. Electrochem. Soc.* **2005**, *152*, A2383–A2389.
(60) Sethuraman, V. A.; Lakshmanan, B.; Weidner, J. W. *Electrochim. Acta* **2009**, *54*, 5492–5499.
(61) Zawodzinski, J. T. A.; Derouin, C.; Radzinski, S.; Sherman, R. J.; Smith, V. T.; Springer, T. E.; Gottesfeld, S. *J. Electrochem. Soc.* **1993**, *140*, 1041–1047.
(62) Hanke-Rauschenbach, R.; Mangold, M.; Sundmacher, K. *Rev. Chem. Eng.* **2011**, *27*, 23–52.
(63) Katsaounis, A.; Tsampas, M.; Balomenou, S. P.; Tsiplakides, D.; Vayenas, C. G. *Solid State Ionics* **2006**, *177*, 2397–2401.
(64) Katsaounis, A.; Balomenou, S. P.; Tsiplakides, D.; Tsampas, M.; Vayenas, C. G. *Electrochim. Acta* **2005**, *50*, 5132–5143.
(65) Vayenas, C. G.; Tsampas, M. N.; Katsaounis, A. *Electrochim. Acta* **2007**, *52*, 2244–2256.
(66) Schneider, I. A.; Bayer, M. H.; Wokaun, A.; Scherer, G. G. *ECS Trans.* **2009**, *25*, 937–948.
(67) Schneider, I. A.; Bayer, M. H.; von Dahlen, S. *J. Electrochem. Soc.* **2011**, *158*, B343–B348.
(68) Schneider, I. A.; Bayer, M.; Wokaun, A.; Scherer, G. *ECS Meet. Abstr.* **2009**, *901*, 1079–1079.
(69) Markovic, N. M.; Grgur, B. N.; Ross, P. N. *J. Phys. Chem. B* **1997**, *101*, 5405–5413.
(70) Markovic, N. M.; Schmidt, T. J.; Grgur, B. N.; Gasteiger, H. A.; Behm, R. J.; Ross, P. N. *J. Phys. Chem. B* **1999**, *103*, 8568–8577.
(71) Sun, Y. B.; Lu, J. T.; Zhuang, L. *Electrochim. Acta* **2010**, *55*, 844–850.
(72) Song, C.; Tang, Y.; Zhang, J. L.; Zhang, J.; Wang, H.; Shen, J.; McDermid, S.; Li, J.; Kozak, P. *Electrochim. Acta* **2007**, *52*, 2552–2561.
(73) Grgur, B. N.; Marković, N. M.; Ross, P. N. *Can. J. Chem.* **1997**, *75*, 1465–1471.
(74) Damjanovic, A.; Sepa, D. B. *Electrochim. Acta* **1990**, *35*, 1157–1162.
(75) Parthasarathy, A.; Dave, B.; Srinivasan, S.; Appleby, A. J.; Martin, C. R. *J. Electrochem. Soc.* **1992**, *139*, 1634–1641.

(76) Paulus, U. A.; Schmidt, T. J.; Gasteiger, H. A.; Behm, R. J. *J. Electroanal. Chem.* **2001**, *495*, 134–145.
(77) Murthi, V. S.; Urian, R. C.; Mukerjee, S. *J. Phys. Chem. B* **2004**, *108*, 11011–11023.
(78) Yano, H.; Higuchi, E.; Uchida, H.; Watanabe, M. *J. Phys. Chem. B* **2006**, *110*, 16544–16549.
(79) Beattie, P. D.; Basura, V. I.; Holdcroft, S. *J. Electroanal. Chem.* **1999**, *468*, 180–192.
(80) Xu, H.; Song, Y.; Kunz, H. R.; Fenton, J. M. *J. Electrochem. Soc.* **2005**, *152*, A1828–A1836.
(81) Pitois, A.; Davies, J. C.; Pilenga, A.; Pfrang, A.; Tsotridis, G. *J. Catal.* **2009**, *265*, 199–208.
(82) Ertl, G.; Neumann, M.; Streit, K. M. *Surf. Sci.* **1977**, *64*, 393–410.
(83) Geng, B.; Cai, J.; Liu, S.-X.; Zhang, P.; Tang, Z.-Q.; Chen, D.; Tao, Q.; Chen, Y.-X.; Zou, S.-Z. *J. Phys. Chem. C* **2009**, *113*, 20152–20155.
(84) Cappadonia, M.; Erning, J. W.; Niaki, S. M. S.; Stimming, U. *Solid State Ionics* **1995**, *77*, 65–69.
(85) Herrero, E.; Álvarez, B.; Feliu, J. M.; Blais, S.; Radovic-Hrapovic, Z.; Jerkiewicz, G. *J. Electroanal. Chem.* **2004**, *567*, 139–149.
(86) Dimitrova, P.; Friedrich, K. A.; Stimming, U.; Vogt, B. *Solid State Ionics* **2002**, *150*, 115–122.
(87) Halim, J.; Büchi, F. N.; Haas, O.; Stamm, M.; Scherer, G. G. *Electrochim. Acta* **1994**, *39*, 1303–1307.
(88) Sone, Y.; Ekdunge, P.; Simonsson, D. *J. Electrochem. Soc.* **1996**, *143*, 1254–1259.